Functional nanostructured chitosan–siloxane hybrids

Simone S. Silva,*[ab] Rute A. S. Ferreira,[c] Lianshe Fu,[c] Luís D. Carlos,[c] João. F. Mano,[ab] Rui L. Reis[ab] and João Rocha[d]

Received 26th April 2005, Accepted 28th June 2005
First published as an Advance Article on the web 26th July 2005
DOI: 10.1039/b505875a

New organic–inorganic hybrids were prepared by a sol–gel method from the biopolymer chitosan and a silane coupling agent, 3-isocyanatopropyltriethoxysilane (ICPTES), in which covalent bridges, essentially composed of urea, bond the chitosan to the poly(siloxane) network. The structural characterization of the advanced chitosan–siloxane hybrids was performed by Fourier transform infrared spectroscopy, X-ray diffraction and ^{29}Si and ^{13}C nuclear magnetic resonance. The presence of siloxane nanodomains was detected by small angle X-ray diffraction. The chitosan–siloxane hybrids are bifunctional materials with interesting photoluminescent features and bioactive behaviour. The photoluminescence spectra display an additional high-energy band with longer lifetime, relatively to the characteristic emission of pure chitosan. This band is associated with electron–hole recombinations arising from silicon-related defects at the surface of the siliceous nanodomains. The bioactive behaviour of these materials was also evaluated; the apatite formation was shown to depend on the amount and arrangement of silanol groups.

Introduction

The development of advanced materials from the combination of macromolecules with inorganic species has become one of the most innovative research fields.[1] Following this approach, the synthesised hybrid materials can allow the tailoring of properties from the atomic to the mesoscopic and macroscopic length scales.[2]

This ability to control materials' properties over broad length scales suggests that research on hybrids can have a significant impact in diverse fields, such as nanoelectronics, separation techniques, catalysis, smart coatings, sensors, immobilization of enzymes, biomedical and polymer composite applications.[1–6] Currently, hybrid materials have been obtained through sol–gel chemistry, which constitutes a versatile method that allows the combination of organic and inorganic or even bioactive components in a single hybrid material.[6–10] In this method, a judicious choice of the constitutive organic and inorganic components as well as reaction parameters (pH, solvent, concentration of the reactants, catalyst, and temperature) allows to tailor the final chemical and physical properties of the materials.[1,2,6] Generally, hybrid materials are grouped in two classes based on the type of interaction or nature of chemical bonding between the organic and inorganic components.[11] In class I the organic component is bonded physically to inorganic phase, whereas in class II hybrids the organic and inorganic compounds are bonded through stronger covalent chemical bonds[11] achieved by using functionalized silanes coupling agents, such as 3-glycidyloxypropyltrimethoxysilane (GPTMS), 3-aminopropyltriethoxysilane (APTES),[12,13] and 3-isocyanatopropyltriethoxysilane (ICPTES). The latter has been used to modify the ethylene vinyl alcohol copolymer[14] and poly(ε-caprolactone-b-perfluoropolyether-b-ε-caprolactone).[7] Recently, the synthesis of amine-functionalized cross-linked sol–gel derived hybrids in which the siliceous backbone is covalently bonded to poly(ether) chains by means of urea or urethane crosslinks originating from ICPTES, named as di-ureasils and di-urethanesils, respectively, have been described.[6,15–21] In particular, the preparation of efficient white-light photoluminescence (PL) siloxane-based organic–inorganic hybrids lacking metal activator ions have been reported.[6,16,18–23] The development of new full colour displays, cheaper and less harmful to the global environment is one of the main challenging tasks for the next generation of flat-panel display systems and lighting technologies.[20] Alternatively to conventional sol–gel process (*e.g.*, in the presence of water and ethanol and inorganic acids as the catalyst), Sailor *et al.*,[12] Lianos *et al.*[13,17] and Carlos *et al.*[15] reported that amine-functionalized sol–gel derived hybrids with attractive photoluminescence features, in particular high emission quantum yields, can also be obtained by a sol–gel derived carboxylic acid solvolysis, which occurs in the absence of water and oxygen, using APTES or ICPTES as silane coupling agents.

A different approach for the preparation of hybrid compounds based on the combination of poly(saccharide)s and silicon-based materials was recently reported.[24–27] In this context, chitosan–siloxane hybrids have received much attention due to their potential for use in enzyme immobilization, porous materials and as electrochemical sensors.[28] Furthermore, chitosan based materials have been proposed

[a]*3Bs Research Group – Biomaterials, Biodegradables and Biomimetics, University of Minho, Campus de Gualtar, 4710-057, Braga, Portugal. E-mail: simonesilva@dep.uminho.pt; Fax: +351 253604492; Tel: +351 2536044781*
[b]*Department of Polymer Engineering, University of Minho, Campus de Azurém, 4800-058, Guimarães, Portugal*
[c]*Department of Physics, CICECO, University of Aveiro, 3810-193, Aveiro, Portugal*
[d]*Department of Chemisty, CICECO, University of Aveiro, 3810-193, Aveiro, Portugal*

 This journal is © The Royal Society of Chemistry 2005

for a range of biomedical applications.[29–31] The methodologies reported focus on the modification of the polymer chain structure before introducing the inorganic component.[32] Alternatively, it is also possible to prepare porous silica particles by elimination of the organic phase (chitosan),[33] or by interaction of chitosan in solution with silica particles to produce aerogel composites,[33,34] films and membranes.[35,36] Devoiselle *et al.*[37] recently reported that porous chitosan–silica hybrid microspheres can be obtained using supercritical drying by CO_2. In these approaches[27,33–37] both organic matrix and inorganic species are physically bonded (class I). It would be interesting to move ahead with this concept by introducing chemical cross-linkages between the reactive groups of chitosan and the siliceous skeleton (class II). If so, a more effective bonding between the organic and the inorganic phases will be achieved, improving the mechanical performance, chemical stability, and controlled water absorption or hydrogel behaviour in a wide pH range. Furthermore, as the optical features of the hybrid materials are significantly affected by the organic/inorganic interfaces, the covalent crosslinkages of these class II poly(saccharide)–siloxane hybrids (urea or urethane groups) may induce optical characteristics distinct from those associated with the class I poly(saccharide)–silicon-based materials.

The main objective of this work was, therefore, to develop novel functional class II poly(saccharide)-based hybrid materials through sol–gel derived carboxylic acid solvolysis. This paper, in fact, reports the first attempt to synthesize a poly(saccharide)-based hybrid material *via* this method. The photoluminescence characterization and a preliminary study of the materials eventual bioactive behaviour are also reported and discussed.

Experimental

Chitosan (Sigma Aldrich medium and low molecular weight) was used as the polymeric component. Molecular viscosimetric weights (Mv = 662 kDa) and (Mv = 591 kDa) were determined in 0.1 M acetic acid–0.2 M sodium acetate as described previously.[38] Before the reaction the polymer was milled to obtain a fine powder. 3-Isocyanatopropyltriethoxysilane (ICPTES), the inorganic constituent, was purchased from Aldrich Chemical Co and used as received. Ethanol (Et, Merck), dimethylformamide (DMF, Merck), acetic acid (AA, Aldrich, 99.7%) were kept in contact with molecular sieves prior to be used.

Synthesis

The chitosan–siloxane hybrids were prepared in two steps using the sol–gel method (Fig. 1). In the first stage, chitosan (fine powder) dispersed in DMF reacted with the silane coupling agent, ICPTES under a N_2 atmosphere during different times (Table 1). In a typical procedure, a sample of 1 g of chitosan (powder) was dispersed under stirring in 10 mL of DMF. Approximately 1.52 mL of ICPTES was added to this dispersion. The flask was sealed and the dispersion was stirred during a pre-determined time (Table 1) at 105 °C under N_2 atmosphere. The reaction was monitored by IR spectroscopy until the characteristic isocyanate band at *ca.* 2274 cm^{-1} vanished. Following the solvolysis process,[17,18] in the second reaction step, an AA–Et mixture in the ratio molar ICPTES : AA : Et of 1 : 3 : 6 and 1 : 6 : 6 was added to the dispersion prepared in step 1. The mixture was stirred in a sealed flask for 24 h at room-temperature in inert atmosphere. The materials were obtained as fine powders. Subsequently, the DMF was separated from the product by centrifugation and washed several times with methanol, after which this solvent was evaporated and the solid allowed to dry overnight in an oven at 60 °C.

Surface modification and *in vitro* apatite forming ability. After washing and the drying of the hybrids, they were also subjected to surface modification using 3 M KOH for 2 h at room temperature. In these tests, the hybrid powders were

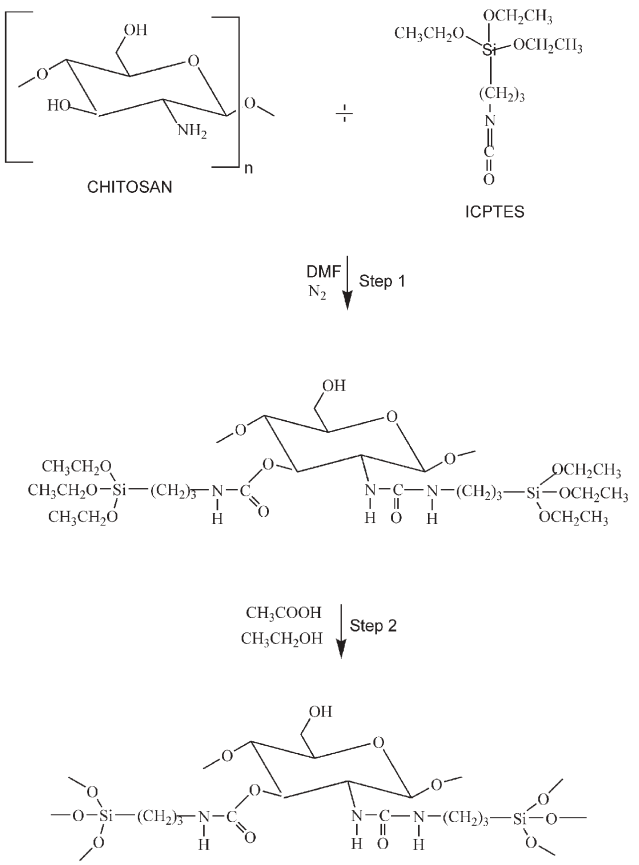

Fig. 1 Scheme proposed for preparation of the chitosan–siloxane hybrids. Although urethane cross-linkages are considered in the scheme urea bridges should be preferentially formed.

Table 1 Experimental synthesis conditions of chitosan–siloxane hybrids[a]

	Molar ratio		Time/h	
Sample	NH_2–NCO	AA–Et	Step 1	Step 2
CHY1	1 : 1.17	3 : 6	48	24
CHY2*	1 : 1.17	3 : 6	48	24
CHY3	1 : 2.34	6 : 6	48	24

[a] CHY1: chitosan hybrid 1; CHY2: chitosan hybrid 2; CHY: chitosan hybrid 3; * hybrid sample obtained from chitosan medium molar viscosimetric weight.

soaked in 10 mL of the simulated body fluid (SBF),[39] at 36.5 °C for a period of up to 21 d to evaluate the bioactivity of the samples by means of looking at the material formation of an apatite-like layer on their surface. Later on, the samples were removed from the fluid, gently rinsed with distilled water and dried at room temperature.

Adsorption measurements. After outgassing the chitosan–siloxane hybrids overnight to a residual pressure of *ca.* 10^{-4} mbar, we have tried (with no success) to measure a nitrogen adsorption isotherm at 77 K. Thus, according to the IUPAC classification the surface area is negligible.

Fourier transform infrared spectroscopy (FT-IR). The FT-IR spectra of KBr pellets were recorded (64 scans with a resolution of 4 cm^{-1}) on a Unican Mattson Mod 7000 FTIR.

Nuclear magnetic resonance (NMR) spectroscopy. ^{29}Si and ^{13}C solid-state NMR spectra were recorded at 79.49 and 100.62 MHz, respectively, on a (9.4 T) Bruker Avance 400 spectrometer. ^{29}Si magic angle spinning (MAS) NMR spectra were measured with 40° rf pulses, a spinning rate of 5.0 kHz, and a recycle delay of 35 s. ^{1}H-^{29}Si cross-polarization (CP) MAS NMR spectra were recorded with 4.0 μs ^{1}H 90° pulses, a spinning rate of 5.0 KHz and 5 s recycle delays. Chemical shifts are quoted in ppm from tetramethylsilane (TMS).

Powder X-ray diffraction (XRD). XRD patterns were recorded on Philips X'Pert MPD diffractometer using Cu Kα radiation (λ = 1.54 Å), 2θ range 1–80°.

Photoluminescence spectroscopy. Emission (PL) and excitation (PLE) photoluminescence spectra and lifetime measurements were recorded between 13 and 300 K on a modular double grating excitation spectrofluorimeter with a TRIAX 320 emission monochromator (Fluorolog-3, Jobin Yvon-Spex) coupled to a R928 Hamamatsu photomultiplier, in the front-face acquisition mode.

Scanning electron microscopy (SEM). SEM images of samples coated with gold were obtained at 10 kV on a Leica Cambridge S-360 microscope equipped with a LINK eXLII X-ray energy dispersion spectrometer for silicon microanalysis.

Small angle X-ray scattering (SAXS). The X-ray scattering measurements were performed in National Synchrotron Light Laboratory (LNLS), Campinas, Brazil, using its SAXS beam line which provides a monochromatic (λ = 1.608 Å) and horizontally focused beam. The intensity was recorded as a function of the modulus of the scattering vector **q**, **q** = $(4\pi/\lambda)\sin(\varepsilon/2)$, ε being the scattering angle. Because of the small size of the incident beam cross section at the detection plane, no mathematical desmearing of the experimental SAXS intensity was needed. Each spectrum corresponds to a data collection period of 300 s. The parasitic scattering intensity from air, slits and windows was subtracted from the total intensity. The scattering intensity was also normalized by taking into account the varying intensity of the direct X-ray beam, sample absorption and sample thickness.

Results and discussion

Structural characterization

Chitosan–siloxane hybrids were prepared through the reaction of the reactive groups of chitosan with the isocyanate group (NCO) of the alkoxysilane precursor, ICPTES (Fig. 1) in the presence of dimethylformamide (DMF), chosen as a dispersing agent. This reaction may produce either urea (–NHCONH–) or urethane (–NHCOO–) groups, which form bridges between the chitosan and the inorganic matrix. The former linkage (–NHCONH–) should be preferentially formed as NH_2 groups react faster with isocyanates than with OH moieties.[40] The formation of chitosan hybrids is summarized in Fig. 1. All reactions were performed in an inert atmosphere to ensure that the ICPTES did not react with moisture. In the second stage of Fig. 1, the hydrolysis and condensation reactions of the precursor occurred with addition of AA and Et in different molar ratios (see Experimental section, Table 1) to yield the corresponding poly(siloxane) Si–O–Si inorganic chain. The two-step reaction mechanism for this process, proposed by Pope and Mackenzie,[41] was recently confirmed by Lianos *et al.* for the AA solvolysis of poly(oxypropylene) 4000–siloxane hybrids in the presence of ethanol using temporal attenuated total reflection IR measurement technique.[17] In the first step, acetic acid reacts with the alkoxy groups bonded to the silicon atom (C_2H_5OSi–), forming an ester (CH_3COOSi–). During the second step, this ester reacts with ethanol, producing ethyl acetate ($CH_3COOC_2H_5$) and Si–OH groups. Then condensation of two Si–OH groups or one Si–OH group and one ethanol molecule yields the Si–O–Si network. The work of De Azevedo and Brondani focused on the development of poly(aniline)–silicate glass composites using formic acid as catalyst and solvent through a sol–gel process also supported this argument.[42]

Hybrid materials obtained by the sol–gel method may present different forms (aerogels, films, xerogels, and powders) depending on the components and preparation conditions.[6] For the particular conditions used in this work (Table 1) it was possible to obtain powdered chitosan–siloxane hybrids. Fig. 2 shows the FTIR spectra of the prepared materials. The displacement of the NH (from 1590 to 1564 cm^{-1}) and CO (from 1652 to 1633 cm^{-1}) deformation bands towards lower wavenumbers provides the evidence for the presence of urea and urethane groups in the hybrids. These shifts, combined with the increase of intensity of the bands, may reflect changes from primary amino groups (chitosan) to urea and urethane

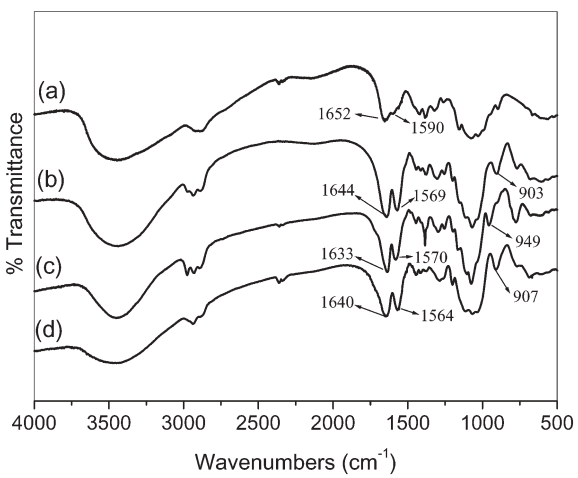

Fig. 2 FTIR spectra of chitosan (a), CHY1 (b), CHY2 (c) and CHY3 (d).

This journal is © The Royal Society of Chemistry 2005

groups. Furthermore, the main IR bands of urea groups overlap with the characteristic absorption bands of chitosan and urethane,[43] making difficult the spectral interpretation. Bermudez *et al.*[15] reported that the "amide I" and "amide II" modes are complex vibrations: amide I (1800–1600 cm^{-1}) involves the contribution of the C=O stretching, C–N stretching, and C–C–N deformation vibrations, while the amide II (1600–1500 cm^{-1}) mode has contributions from the N–H in plane bending, C–N stretching, and C–C stretching vibrations. In order to study in detail the vibrations for the urea and urethane groups spectral deconvolutions were carried out in the 1800–1500 cm^{-1} range using the ORIGIN® package and Gaussian band shapes. The results are listed in Table 2.

According to the literature, the components at *ca.* 1690 and 1655 cm^{-1} are tentatively due to the vibration of urea–poly(ether) hydrogen-bonded structures, whereas the component at about 1630 cm^{-1} results from the formation of strong self-associated hydrogen-bonded urea–urea associations.[15,18] The absence in the spectra of Fig. 2 of an individual band at *ca.*1750 cm^{-1} indicates that neither C=O nor N–H groups are left free (with no hydrogen bond interactions), in agreement with that reported before for di-ureasils with shorter polymer chains.[15,18] However, for di-urethanesil hybrids the "amide I" envelope involves essentially three bands, at *ca.* 1750, 1720 and 1696 cm^{-1}, ascribed to urethane linkages in which the N–H and C=O groups are nonbonded, hydrogen-bonded C=O groups in poly(ether)–urethane associations, and C=O groups belonging to a considerably more ordered hydrogen-bonded urethane–urethane disordered aggregates, respectively.[18,19] Therefore, the band at *ca.* 1680–1696 cm^{-1} in Table 2 could be associated both to urea–poly(ether) hydrogen-bonded structures and urethane–urethane hydrogen-bonded associations. However, the urea cross-linkages may exist in larger amounts in accordance with previously observations indicating that NH_2 groups react much more rapidly with isocyanates than OH moieties.[40]

The inorganic phase gives IR bands in the following regions: 1100–1000, 950–900 and 800–700 cm^{-1} assigned, respectively, to Si–O–Si (stretch mode), Si–OH (stretch mode) and Si–O–Si.[15,44] The presence of residual silanol (Si–OH) groups is a common situation in many sol–gel derived materials, reflecting incomplete polycondensation.[15] The chitosan spectrum (Fig. 2a) displays a band at 1100–1000 cm^{-1}, attributed to –C–O–C– of glycosidic linkage.[43] In the hybrids spectra (Fig. 2b–e) this band increases intensity, possibly due to the overlapping of the Si–O band in the same frequency region.

Fig. 3 shows the ^{13}C CP/MAS NMR of chitosan and derivatives. In the spectra of the hybrids (Fig. 3b–d), the bridge

Table 2 Curve-fitting results of "amide I" and "amide II" regions in the FT-IR spectra of CHY1, CHY2, and CHY3

Sample	CHY 1	CHY2	CHY3
"Amide I"			
Wavenumber/cm^{-1} (area)	1689 (36%)	1696 (33%)	1680 (19%)
	1654 (48%)	1656 (39%)	1651 (25%)
	1629 (16%)	1632 (28%)	1643 (56%)
Amide II			
Wavenumber/cm^{-1}	1572	1579	1568

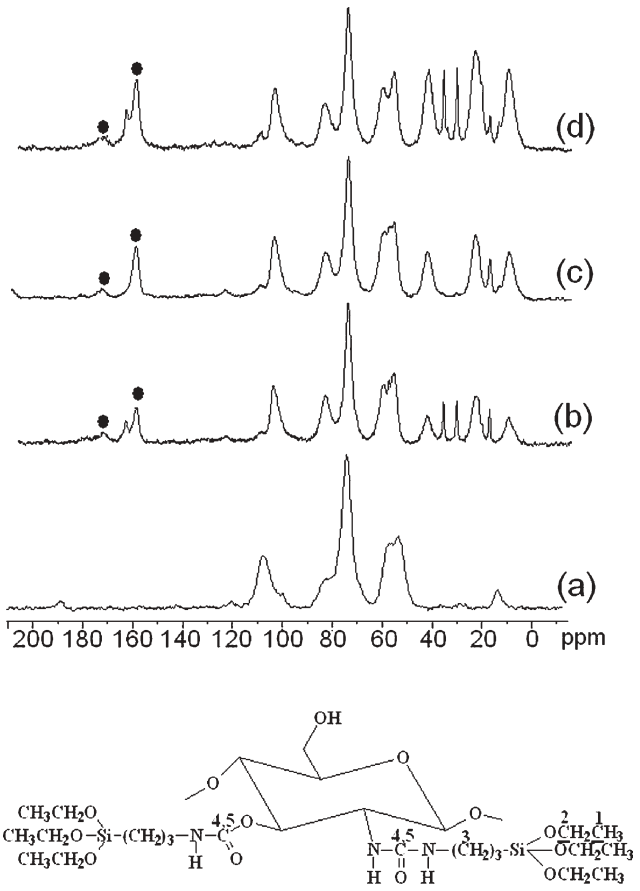

Fig. 3 ^{13}C CP MAS of chitosan (a), CHY1 (b), CHY2 (c) and CHY3 (d).

of the siloxane network to the polymer is confirmed by the appearance of new signals at *ca.* 23, 43 and 160–170 ppm. The peaks at *ca.* 23 and 43 ppm are given by the ester group (C_1, C_2) carbons bonded to silicon atom (–SiOCH_2CH_3) and the aliphatic $(CH_2)_3$ carbons of the silane precursor (C_3), respectively (see Fig. 3). In addition, the intensity of the peak at *ca.* 18 ppm increases, as a result of the overlapping of the resonances of the methyl groups of the polymer chain[45] with the resonances of the CH_3 of ethoxy (OCH_2CH_3) groups. Furthermore, the ^{13}C CP/MAS NMR spectra exhibit several resonances at *ca.* 160–170 ppm ($C_{4,5}$) that are associated with carbonyl groups in different environments.[18,19,46] This supports the hypothesis that urea and urethane bridges may coexist in the hybrids. The prepared chitosan–siloxane derivatives are thus bifunctional hybrids, forming an interconnected network with the inorganic component through urea (essentially) and urethane bridges. Hence, the chitosan (amino and hydroxyl groups) functionality offers different ways of obtaining class II hybrid materials.

Solid-state ^{29}Si MAS NMR spectroscopy is a useful technique to elucidate the structure of hybrid materials. The ^{29}Si MAS NMR spectra of the hybrids studied here (Fig. 4) exhibit broad signals in three distinct regions, *ca.* −48 to −50, −58 to −59 and −66 to −68 ppm, assigned to T_1, T_2 and T_3 environments, respectively.[6,18,19,21] The silicon sites are labelled according to the conventional T_n notation,

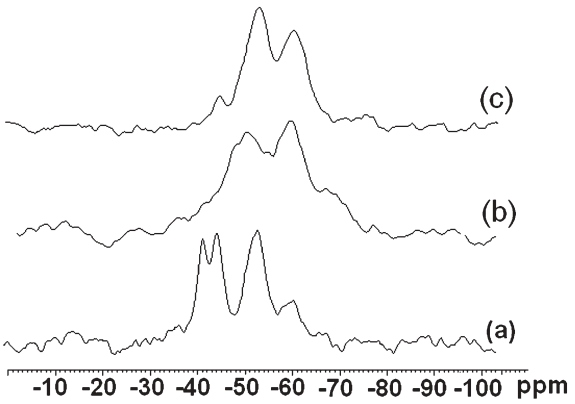

Fig. 4 ^{29}Si MAS NMR spectra for CHY1 (a), CHY2 (b) and CHY3 (c).

where n (n = 1, 2, 3) is the number of Si-bridging oxygen atoms. As the sol–gel process progresses, new peaks associated with the formation of the siloxane (–Si–O–Si–) and/or Si–OH groups appear. The signals from T_2 sites are stronger than the signals given by the T_3 environments for CHY1, CHY2 and CHY3 samples (Fig. 4). This suggests that partial condensation favours lightly branched structures rather than linear segments. The intensity of the CHY3 peaks at *ca.* −66.7 and *ca.* −58 ppm increases, while it decreases for the *ca.* −48.6 ppm resonance, confirming that a large population of siloxane groups is present in this hybrid. The degree of condensation (c) involves the population (intensity) of the distinct Si (T_1, T_2, T_3) environments and it was calculated using the equation c = 1/3 ($\%T_1$ + $2\%T_2$ + $3\%T_3$).[18,21] The peak assignment and the relative populations of the different Si sites, estimated after deconvolution using Gaussian band shapes, are depicted in Table 3. The results show that the degree of poly(siloxane) formation in each hybrid is different, depending on the experimental conditions. The increase of isocyanate and AA–Et molar ratio in CHY3 (refer to the Experimental section) increases the population of the T_2 and T_3 sites and reduces the population of the T_1 site, leading to a higher degree of condensation (71%) and, hence, a close network structure is formed. The change of the molecular weight of chitosan used to prepare CHY2 did not significantly change the degree of condensation. In general, the results confirm that the siloxane network was incorporated, to different extents, into chitosan.

It was worth noting that the variation of the polycondensation degree with the NCO : NH_2 ratio (Table 3) agrees well with the deconvolution of the "amide I" region (Table 2). The larger ratio of NCO : NH_2 results in more precursors formed in the first step and more complete polycondensation in the second step and consequently higher degree of condensation. This is consistent with the decrease of the amount of urea–polyether hydrogen-bonded structures and the simultaneous increase of the amount of strong self-associated hydrogen-bonded urea–urea associations as the NCO : NH_2 ratio enlarges (Table 2).

Table 3 ^{29}Si NMR chemical shifts and population of the different T_n species and degree of condensation, c, of the chitosan–siloxane hybrids

Sample	CHY 1	CHY2	CHY3
Precursor	−45.3 (26)	−45.6 (18)	—
T1– $Si(OSi)(OR)_2$ (%)	−49.9 (29)	−49.8 (26)	−48.6 (15)
T2– $R'Si(OSi)_2(OR)$ (%)[a]	−58.2 (35)	−57.9 (45)	−58.0 (58)
T3– $R'Si(OSi)_3$ (%)	−65.7 (10)	−66.0 (11)	−66.7 (27)
c (%)[b]	43	50	71

[a] R denotes the ethoxy groups; R′denotes the polymeric chain bonded to urea groups; [b] c = degree of condensation; in parenthesis is the population.

The room temperature powder X-ray diffraction patterns of chitosan and chitosan–siloxane hybrids are shown in Fig. 5a. All the patterns exhibit a main peak centred at *ca.* 20.02° associated with the chitosan crystalline structure.[47] The second-order of this peak appears as a broad hump at *ca.* 40°. Accordingly, a structural unit distance of 4.43 ± 0.1 Å is obtained. For the chitosan–siloxane hybrids, both peaks broaden due to the presence of siloxane nanodomains, whose first diffraction peak appears at *ca.* 21.0–21.7°.[6,18–20] For instance, in the pattern of the CHY1 chitosan–siloxane hybrid the full-width-at-half-maximum (fwhm) of the main peak increases *ca.* 50%, relatively to the fwhm of this peak in the chitosan matrix pattern.

In addition, a shoulder is clearly observed at *ca.* 10° in the trace of pure chitosan. This feature is ascribed to other type of ordering within the chitosan chains, with a characteristic distance of *ca.* 8.5 ± 0.3 Å. For the chitosan–siloxane hybrids, this peak is not seen, and two broad and weak humps are present at *ca.* 8.5–9.0 and 12.0–12.5°.

The peak appearing at low angles, *ca.* 5°, in the XRD patterns of chitosan–siloxane hybrids (inset of Fig. 5a) is ascribed to interparticle scattering interference and indicates a

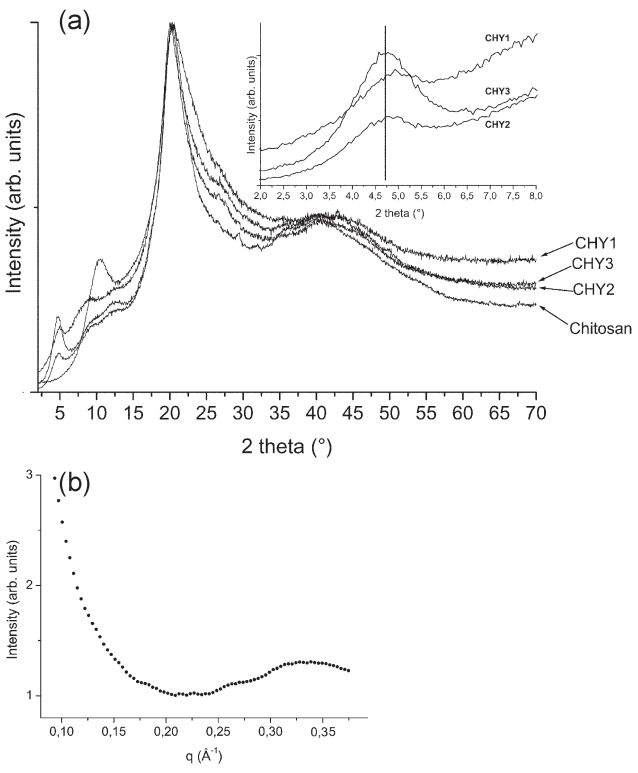

Fig. 5 (a) Powder X-ray diffraction patterns of chitosan–siloxane hybrids. The inset shows the XRD diffractograms in the low 2θ region. (b) SAXS pattern of the CHY3 chitosan–siloxane hybrid.

This journal is © The Royal Society of Chemistry 2005

highly non-periodic fluctuation of the electronic density in these hybrid materials. This well-defined peak, which is also clearly seen in the SAXS scattering profile of the CHY3 hybrid (Fig. 5b), was attributed to the liquid-like spatial correlation of siloxane-rich domains embedded in the polymer matrix and located at the ends of the organic segments.[48,49] This result suggests a diphasic structure for the morphology of the hybrids caused by local phase separation between inorganic silicon-rich domains and polymeric regions, as in the case of analogous di-ureasil and di-urethanesil hybrids.[6,18–23]

From the XRD peak maximum position (Fig. 5a) the average interparticle distance, d, is estimated to be 18–19 $\pm$ 1 Å. From the magnitude of the SAXS scattering vector of the peak maximum, the corresponding interdomain distance is calculated as d = 18.6 $\pm$ 0.1 Å, matching well the value extracted from the XRD diffractogram. This distance is similar to that reported for similar organic–inorganic hybrids.[6,48,49]

In vitro apatite forming ability

It is known that the presence of Si–OH groups in different types of materials can induce the formation of a bone-like apatite layer.[50–52] In the present work preliminary *in vitro* apatite forming ability tests in simulated body fluid (SBF) were conducted to assess the ability of the chitosan hybrids to induce the formation of an apatite layer on its surface. Pure chitosan did not show ability to induce the apatite formation (Fig. 6a). For chitosan–siloxane hybrids, the formation of

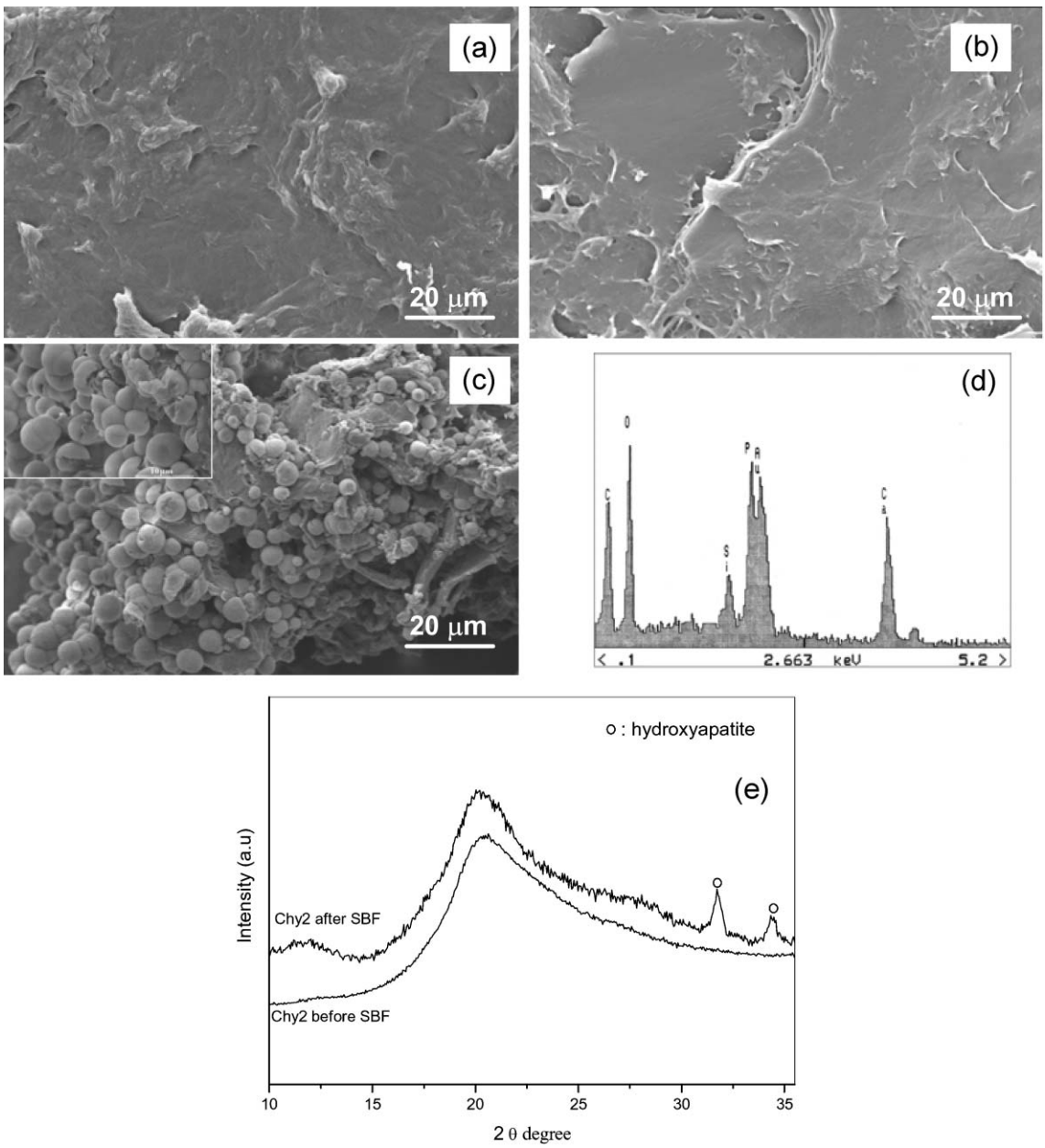

Fig. 6 SEM images of the chitosan (a), CHY2 before immersion in SBF (b), CHY2 after 21 d in immersion in SBF (c), EDS analysis (d), and XRD analysis (e).

Ca–P nuclei sitting on specific sites of the substrate surface was observed. It can be seen that the formation of precipitates occurs, which may be due to the apatite formation (Fig. 6c) after immersion in SBF for 21 d. The EDS analysis revealed that the precipitates consisted of calcium and phosphorus elements (Fig. 6d). Fig. 6e shows the XRD results for chitosan–siloxane hybrids after soaking in SBF. It can be observed that apatite peaks were observed after immersion in SBF on the surface of CHY2 sample. The diffraction peaks above 30° in the XRD spectra are in agreement with the standard pattern of hydroxyapatite (JCPDS 9-432), although the partially amorphous nature of film was also evident. These results are in agreement with the ones obtained from SEM, where only apatite nuclei were observed on the surface of hybrid (seen by Fig. 6c). The results indicate that a longer soaking period (21 d) is required to form Ca–P nuclei, and this effect depends on the amount and arrangement of silanol groups in the materials structure. The results in this work suggest that such systems do in fact exhibit a bioactive behaviour. However, further improvements in the compositions, synthesis conditions and surface modification, would be necessary to minimise the time necessary to observe the apatite layer formation.

Photoluminescence

Figs. 7 show the excitation (PLE) spectra of chitosan and two representative chitosan–siloxane hybrids (CHY1 and CHY3).

The low-temperature chitosan spectrum consists of a large broad band between 240 and 420 nm, where it is possible to discern a main component, whose peak position occurs at *ca.* 375 nm, and two lower intensity bands, located at *ca.* 290 and 335 nm. Marked changes are observed in the low-temperature PLE spectra of the chitosan–siloxane hybrids, particularly in the high-energy region. These spectra are formed by two main peaks at *ca.* 245 and 278 nm and by a lower intensity broad band region showing two main components at *ca.* 335 and 375 nm, similarly to what was observed in the chitosan spectrum. The main differences observed between the PLE features of the two hybrids are in the relative intensity of the two peaks (245 and 278 nm) and in the higher contribution of the band centred around 335 nm for the CHY3 PLE spectrum.

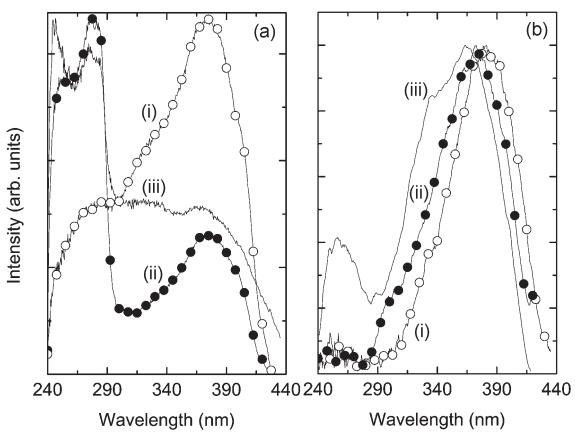

Fig. 7 PLE spectra of chitosan (i), CHY1 (ii), and CHY3 (iii), monitored around 440–450 nm at 13 (a) and 300 K (b).

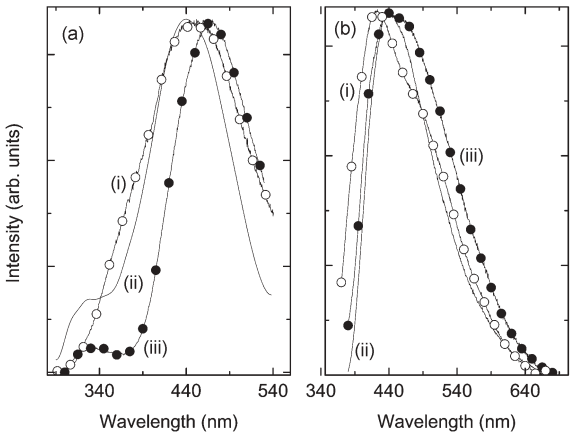

Fig. 8 PL spectra measured at 13 K of chitosan (i), CHY1 (ii), and CHY3 (iii) excited at 278 (a) and 375 nm (b).

Raising the temperature to 300 K, all the spectra display a main band peaking around 362–378 nm, and only the spectrum of the CHY3 hybrid shows a lower intensity band at *ca.* 256 nm.

Figs. 8 present the low-temperature emission (PL) spectra of chitosan and CHY1 and CHY3 hybrids recorded at two selected excitation wavelengths (278 and 375 nm). For the lower excitation wavelength (Fig. 8a), all the spectra display a large broad band peaking around 450–480 nm. For the hybrids it is also possible to clearly discern another lower-intensity component around 340 nm. For 375 nm excitation wavelength, all the spectra display a large broad band at *ca.* 450–480 nm. Comparing the PL features of CHY1 and CHY3, there is a red-shift of the more intense band of the latter hybrid, whereas the more energetic emission has a greater contribution to PL spectra of the former hybrid.

At room temperature the band around 340 nm could not be detected. Apart from an intensity reduction around 30% the spectra display only the lower energetic broad band that has been detected at 13 K (Fig. 8b).

Preliminary lifetime measurements were carried out at 13 K for the chitosan and chitosan–siloxane hybrids (not shown). The lifetimes were monitored around 455–472 nm under 284–300 nm excitation wavelength with a starting delay of 0.05 ms. For such experimental conditions the data reveal a non-single exponential behaviour and therefore an effective lifetime (τ_e) for which the PL intensity is reduced to 1/*e* of its maximum intensity was considered. The τ_e values found for the CHY1 and CHY3 are around 350 ms and for the pure chitosan a faster τ_e of *ca.* 90 ms was estimated. At room temperature both the hybrids' and the chitosan's emission bands have lifetimes faster than the limit detection of our experimental equipment (0.050 ms).

The hybrids' emission strongly depends on the excitation wavelength, over the whole temperature range between 13 and 300 K. Fig. 9 shows the low temperature spectra of the CHY3 hybrid for the excitation range between 350 and 420 nm. A blue-shift of the emission energy and an increase in the fwhm with the decrease of the excitation wavelength are observed. The energy dependence on the excitation wavelength has already been discussed for analogous poly(oxyethylene)

 This journal is © The Royal Society of Chemistry 2005

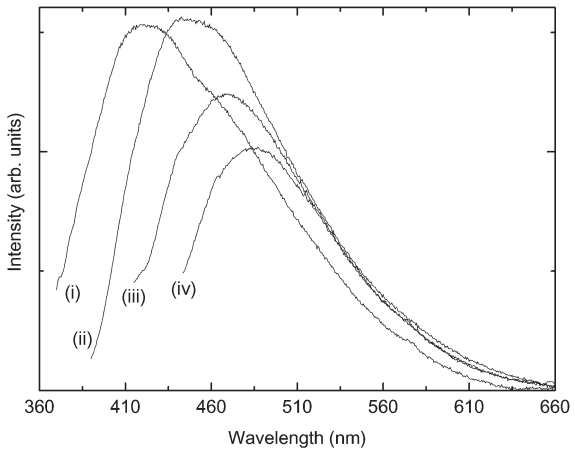

Fig. 9 PL spectra measured at 13 K of CHY3 hybrid excited at (i) 350, (ii) 375, (iii) 400 and (iv) 420 nm.

(PEO)–siloxane and poly(oxypropylene) (POP)–siloxane hybrids,[6,17–23] providing strong evidence of disorder-related processes, which are generally associated with transitions between localized states in amorphous structures. The origin of such behaviour is probably connected with radiative electron–hole recombinations involving localized states within the conduction and valence bands.[6,20,21]

The previous results for the chitosan–siloxane hybrids, namely the presence of more than one PLE component and the increase in the fwhm of the PL spectra as the excitation wavelength decreases from 420 to 350 nm strongly suggest the presence of more than one emission component. In order to further interpret the PL features a deconvoluting fitting procedure was applied to the emission spectra of the chitosan–siloxane hybrids, in the excitation wavelength range between 330 and 420 nm. The used method was similar to that reported for other classes of organic–inorganic hybrids such di-ureasils and di-urethanesils.[6,18,20,21] One Gaussian function was used to fit the emission spectrum excited within the interval 400–420 nm (2.95–3.10 eV). Since the fwhm is determined primarily by carrier–photon interaction, its value should not be affected by the variation of the excitation energy.[6,18,20] Therefore, for each hybrid, the fwhm-fitted values were considered to be independent of the excitation energy. In contrast, the peak energies and their integrated intensity were, for each hybrid, free to vary for the whole excitation energy range used. For excitation wavelengths between 330 and 375 nm (3.31–4.00 eV) the fitting method revealed the presence of two Gaussian bands in the blue (*ca.* 2.53–2.64 eV) and in the purplish-blue (*ca.* 2.82–3.12 eV) spectral regions. Only the former component was observed for excitation wavelengths in the 400–420 nm (2.95–3.10 eV) interval. The fwhm reached approximately 0.50 and 0.35 eV for the blue and purplish-blue bands, respectively. It was observed that the energy of the blue band is almost independent of the excitation wavelength, whereas the energy of the purplish-blue band shifts to the red as the excitation wavelength decreases.

Comparing these fit results with those already reported for other classes of analogous organic–inorganic hybrids, such as di-ureasils and di-urethanesils, we can ascribe the origin of the blue and purplish-blue components to electron-hole recombinations that occur in the NH groups and in the siloxane nanoclusters, respectively. For the di-ureasils and di-urethanesils, it has been recently demonstrated that these two components reveal a radiative recombination mechanism typical of donor–acceptor pairs, mediated by some localized centers.[21] Photoinduced proton-transfer between defects such as NH_2^+ and N^- is proposed as the mechanism responsible for the NH-related component.

The chitosan-related emission might be originated by electron–hole recombinations that take place in the NH groups, similar to the blue band in the chitosan–siloxane hybrids.

Returning to the fit results, the most notorious variations found in the fitting parameters are related with variations in the integrated intensity of the two PL components. The data in Fig. 10 show that the relative contribution between the integrated intensity of the NH and siliceous-related emissions strongly depends on the sample. For the CHY1 hybrid it is observed that the NH emission component dominates the overall emission independent on the selected excitation wavelength within the interval 330–400 nm. For CHY3 the previous results occur only for excitation wavelengths higher than 350 nm, since at lower excitation wavelengths (350–330 nm) the PL associated with the siliceous domains dominates the emission features. Such range of excitation wavelengths favours the siliceous related emission, so that an increase in the emission intensity observed for the CHY3 sample with respect to the NH-related emission might be a consequence of the higher condensation degree of this hybrid (the number of defects associated with the dangling bonds, for instance, increases with the condensation degree), see Table 3.

The smaller contribution of the NH groups to the PL features of the CHY3 hybrid relatively to the CHY1 may be induced by the stronger hydrogen bonds established between

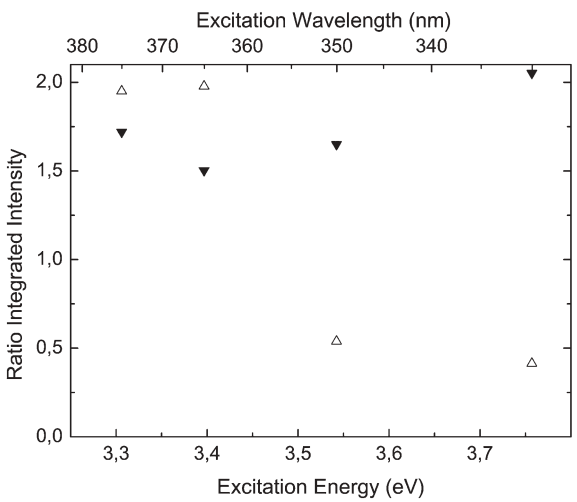

Fig. 10 RT ratio of the integrated intensity of the NH (blue band) and siliceous (purplish-blue band) related emission for the CHY1 (down triangle) and CHY3 (up triangle) hybrids, obtained from the fit procedure to the PL spectra obtained at different excitation wavelengths.

adjacent urea groups, as pointed out by FTIR results (Table 2). The presence of stronger hydrogen bonds in CHY3 contributes to localize the proton rendering difficult its induced transfer between NH groups and, consequently, reducing the intensity of the NH-related emission.

Conclusions

Poly(saccharide)–inorganic hybrids based on low-molecular weight chitosan are interesting because of their chemical versatility, which allows tailoring novel functionalities accomplished by linkages between the different polymer groups and the inorganic components. Novel chitosan–siloxane hybrids were synthesized by a sol–gel derived carboxylic acid solvolysis. Structural characterization by a range of techniques (FTIR, ^{29}Si MAS NMR, ^{13}C CP/MAS NMR, powder XRD, SEM) confirmed that the derivatives are bifunctional hybrids, in which urea and urethane bridges covalently bond chitosan to the poly(siloxane) network. From the bioactivity tests, it can be concluded that the apatite formation mainly depends on the amount and arrangement of the silanol groups in materials structure. The PL results furnish unequivocal evidence for the presence of a new band with higher energy and long lifetime, relatively to the characteristic emission of pure low-molecular weight chitosan. Since this component is associated with electron–hole recombinations mediated by donor–acceptor pairs arising from oxygen-related defects at the surface of the siliceous nanodomains (dangling bonds, for instance), the features observed in the high-energy region of the PL spectrum of CHY3, relatively to the remaining hybrids, could be connected with the higher condensation degree of their inorganic domains (Table 3) and with the stronger hydrogen bonds established between adjacent urea groups (Table 2) . The siloxane–chitosan hybrids therefore exhibit interesting photoluminescence characteristics that may be suitable for their use as optical probes for applications *in vivo*.

Acknowledgements

The authors thank the Anabela Valente (CICECO, University of Aveiro) and Verónica de Zea Bermudez (UTAD) for their help on the adsorption measurements and synthesis process, respectively. L.D. Carlos acknowledges Karim Dahmouche (UNESP, Brazil), Nuno Silva (CICECO, University of Aveiro) and LNLS staff for their collaboration during SAXS experiments/analysis. S.S. Silva and L. Fu thank the Portuguese Foundation for Science and Technology (FCT) for providing PhD and postdoctoral scholarships (SFRH/BD/8658/2002 and SFRH/BPD/5657/2001, respectively). This work was partially supported by FCT, through funds from the POCTI and/or FEDER programmes.

References

1 *Functional Hybrid Materials*, ed. P. G. Romero and C. Sanchez, Wiley-VCH, Weinheim, 2003.
2 C. Sanchez, G. J. D. A. A. Soler-Illia, F. Ribot and D. Grosso, *C. R. Chim.*, 2003, **6**, 1131.
3 B. Lebeau and C. Sanchez, *Curr. Opin. Solid State Mater. Sci.*, 1999, **4**, 11.
4 C. Sanchez and B. Lebeau, *Mater. Res. Soc. Bull.*, 2001, **26**, 377.
5 M. Messori, M. Toselli, F. Pilati, L. Mascia and C. Tonelli, *Eur. Polym. J.*, 2002, **38**, 1129.
6 L. D. Carlos, R. A. Sá Ferreira and V. de Zea Bermudez, *Handbook of Organic–Inorganic Hybrid Materials and Nanocomposites*, ed. H. S. Nalwa, American Scientific Publishers, California, 2003, **vol. 1**, ch. 9, p. 353.
7 J. C. Biazzotto, H. C. Sacco, K. J. Ciuffi, A. G. Ferreira, O. A. Serra and Y. Iamamoto, *J. Non-Cryst. Solids*, 2000, **273**, 186.
8 X. Y. Shang, Z. K. Zhu, J. Yin and X. D. Ma, *Chem. Mater.*, 2002, **14**, 71.
9 J. J. E. Moreau, L. Vellutini, M. Wong Chi Man and C. J. Bied, *J. Am. Chem. Soc.*, 2001, **123**, 1509.
10 T. Coralin, E. Mercey, L. Linsnard and J. Livage, *Chem. Commun.*, 2001, **23**, 2496.
11 C. Sanchez and F. Ribot, *New J. Chem.*, 1994, **18**, 1007.
12 W. H. Green, K. P. Le, J. Grey, T. T. Au and M. J. Sailor, *Science*, 1997, **276**, 1826.
13 (*a*) V. Bekiari and P. Lianos, *Langmuir*, 1998, **14**, 3459; (*b*) V. Bekiari and P. Lianos, *Chem. Mater.*, 1998, **10**, 3777.
14 L. Ren, K. Tsuru, S. Hayakawa and A. Osaka, *J. Sol–Gel Sci. Technol.*, 2001, **21**, 115.
15 V. de Zea Bermudez, L. D. Carlos and L. Alcácer, *Chem. Mater.*, 1999, **11**, 569.
16 E. Stathatos, P. Lianos, U. L. Stangar and B. Orel, *Adv. Mater.*, 2002, **14**, 354.
17 V. Bekiari, P. Lianos, U. L. L. Stangar, B. Orel and P. Judenstein, *Chem. Mater.*, 2000, **12**, 3095.
18 L. Fu, R. A. Sá Ferreira, M. J. O. Silva, L. D. Carlos, V. de Zea Bermudez and J. Rocha, *Chem. Mater.*, 2004, **16**, 1507.
19 M. C. Gonçalves, V. de Zea Bermudez, R. A. Sá Ferreira, L. D. Carlos, D. Ostrovskii and J. Rocha, *Chem. Mater.*, 2004, **16**, 2530.
20 L. D. Carlos, V. de Zea Bermudez, R. A. Sá Ferreira, L. Marques and M. Assunção, *Chem. Mater.*, 1999, **11**, 581.
21 L. D. Carlos, R. A. Sá Ferreira, I. Orion, V. de Zea Bermudez and J. Rocha, *J. Lumin.*, 2000, **702**, 87.
22 L. D. Carlos, R. A. Sá Ferreira, V. de Zea Bermudez and S. J. L. Ribeiro, *Adv. Funct. Mater*, 2001, **2**, 111.
23 L. D. Carlos, R. A. Sá Ferreira, R. N. Pereira, M. Assunção and V. de Zea Bermudez, *J. Phys. Chem. B.*, 2004, **108**, 14924.
24 L. Ren, K. Tsuru, S. Hayakawa and A. Osaka, *J. Sol–Gel Sci. Technol.*, 2001, **21**, 115.
25 Y. A. Shchipunov, *J. Colloid Interface Sci.*, 2003, **268**, 68.
26 S. Fuentes, P. J. Retuert, A. Ubilla, J. Fernandez and G. Gonzalez, *Biomacromolecules*, 2000, **1**, 239.
27 J. Retuert, R. Quijada, V. Arias and M. Y. Pedram, *J. Mater. Res.*, 2003, **18**, 487.
28 R. Bond and J. C. McAuliffe, *Aust. J. Chem.*, 2003, **56**, 7.
29 S. S. Silva, M. I. Santos, O. P. Coutinho, J. F. Mano and R. L. Reis, *J. Mater. Sci.: Mater. Med.*, 2005, **16**, 575.
30 K. Tuzlakoglu, C. M. Alves, J. F. Mano and R. L. Reis, *Macromol. Biosci.*, 2004, **4**, 811.
31 E. T. Baran, K. Tuzlakoglu, A. J. Salgado and R. L. Reis, *J. Mater. Sci.*, 2004, **15**, 161.
32 A. P. Zhu, Z. Zhang and J. Shen, *J. Mater. Sci.*, 2003, **14**, 27.
33 M. R. Ayers and A. Hunt, *J. Non-Cryst. Solids*, 2001, **285**, 123.
34 X. Hu, K. Littrel, S. Ji, D. G. Pickles and W. M. Rinsen, *J. Non-Cryst. Solids.*, 2001, **288**, 184.
35 S. Park, J. O. You, H. Y. Park, S. J. Haam and W. S. Kim, *Biomaterials*, 2001, **22**, 323.
36 C. Airoldi and O. A. C. Monteiro, *J. Appl. Polym. Sci.*, 2000, **77**, 797.
37 K. Molvinger, F. Quignard, D. Brunel, M. Boissière and J. M. Devoisselle, *Chem. Mater.*, 2004, **16**, 3367.
38 R. A. A. Muzzarelli and M. G. Peter, *Chitin Handbook*, European Chitin Society, Atec, Grottammare, 1997, ch. 3, p. 109.
39 T. Kokubo, H. Kushitani, S. Sakka, T. Kitusgi and T. Yamamuro, *J. Biomed. Mater. Res.*, 1990, **24**, 721.
40 P. V. Morales, J. F. L. Nest and A. Gandini, *Electrochimica Acta*, 1998, **43**, 1275.
41 E. J. Pope and J. D. Mackenzie, *J. Non-Cryst. Solids*, 1986, **87**, 185.

 This journal is © The Royal Society of Chemistry 2005

42 W. M. D. Azevedo and D. J. Brondani, *J. Non-Cryst. Solids*, 2001, **296**, 224.
43 A. Pawlak and M. Mucha, *Thermochim. Acta*, 2003, **396**, 153.
44 A. Bertoluzza, C. Fagnano, M. A. Morelli, V. Gottardi and M. Guglielmi, *J. Non-Cryst. Solids.*, 1982, **48**, 117.
45 O. A. C. Monteiro and C. Airoldi, *Int. J. Biol. Macrom.*, 1999, **26**, 119.
46 A. C. Franville, R. Mahiou, D. Zambon, Y. Troin and J. C. Cousseins, *Solid State Sci.*, 2001, **3**, 211.
47 M. Jaworska, K. Sakurai, P. Gaudon and E. Guibal, *Polym. Int.*, 2003, **52**, 198.
48 K. Dahmouche, C. V. Santilli, S. H. Pulcinelli and A. F. Craievich, *J. Phys. Chem. B*, 1999, **103**, 4937.
49 K. Dahmouche, L. D. Carlos, V. de Zea Bermudez, R. A. Sá Ferreira, C. V. Santilli and A. F. Craievich, *J. Mater. Chem.*, 2001, **11**, 3249.
50 T. Kokubo, H. M. Kim and M. Kawashita, *Biomaterials*, 2003, **24**, 2161.
51 S. H. Rhee, *Biomaterials*, 2003, **24**, 1721.
52 A. Oyane, K. Nakanishi, H. M. Kim, F. Miyaji, T. Kokubo, N. Soga and T. Nakamura, *Biomaterials*, 1999, **20**, 79.

This journal is © The Royal Society of Chemistry 2005